Effect of impurities on the transition between minority ion and mode conversion ICRH heating in (^{3}He)–H tokamak plasmas

Ye.O. Kazakov[1], T. Fülöp[1] and D. Van Eester[2]

[1] Department of Applied Physics, Nuclear Engineering, Chalmers University of Technology and Euratom-VR Association, Göteborg, Sweden
[2] LPP-ERM/KMS, Association Euratom-'Belgian State', TEC Partner, Brussels, Belgium

E-mail: `kazakov@chalmers.se`

Abstract. Hydrogen majority plasmas will be used in the initial non-activated phase of ITER operation. Optimizing ion cyclotron resonance heating (ICRH) in such scenarios will help in achieving H-mode in these plasmas. Past JET experiments with the carbon wall revealed a significant impact of intrinsic impurities on the ICRH performance in (^{3}He)–H plasmas relevant for the full-field initial ITER phase. High plasma contamination with carbon impurities resulted in the appearance of a supplementary mode conversion layer and significant reduction in the transition concentration of ^{3}He minority ions, defined as the concentration at which the change from minority heating to mode conversion regime occurs. In view of the installation of the new ITER-like wall at JET, it is important to evaluate the effect of Be and W impurities on ICRH scenarios in (^{3}He)–H plasmas. In this paper, an approximate analytical expression for the transition concentration of ^{3}He minority ions is derived as a function of plasma and ICRH parameters, and accounting for typical impurity species at JET. The accompanying 1D wave modeling supports the analytical results and suggests a potential experimental method to reduce ^{3}He level needed to achieve a specific heating regime by puffing a small amount of ^{4}He ions additionally to (^{3}He)–H plasma.

PACS numbers: 52.25 Fi, 52.25 Ya, 52.55 Fa

1. Introduction

Ion cyclotron resonance heating (ICRH) has been used successfully for bulk ion and electron heating in tokamaks, and is foreseen as one of the additional heating systems to be installed at ITER. At the initial stage of ITER operation predominantly hydrogen (H) or helium-4 (^{4}He) plasma will be used to minimize the activation of the tokamak components [1]. The existing scalings suggest the H-mode power threshold to be higher by a factor of two for hydrogen plasmas than for deuterium, and therefore the access to H-mode of operation is not assured for H plasmas in ITER with the heating powers that will be available [2]. Thus, it is particularly important to optimize the efficiency of radio frequency (RF) heating for the scenarios relevant for this experimental stage of ITER.

It is well known that for efficient ICRH heating at the fundamental ion cyclotron (IC) frequency plasmas consisting of at least two different ion species need to be used. The concentration of one ion species (majority) is usually much higher than the concentration of another species (minority ions). Depending on the relative concentrations of the species, two heating regimes are usually identified: minority ion heating (MH) and mode conversion (MC). MH requires relatively low minority concentrations, less than some critical value [3]. In this regime the majority ions assure favourable polarization of the fast Alfvén wave (FW) launched by the ICRH antenna at the region of the fundamental cyclotron resonance of minority ions, which absorb the RF energy and transfer it to bulk plasma ions and electrons via Coulomb collisions. Whether indirect bulk ion or electron heating dominates, depends on the ratio between the minority tail energy and the critical energy, $E_{\rm crit}$ [4]. When the averaged energy of the fast minority ions is above $E_{\rm crit}$ electrons are predominantly heated by collisions with the fast ions, whereas for the opposite case indirect bulk ion heating is observed. With the gradual increase in the minority concentration the MH efficiency reduces and at large enough minority concentrations plasma heating via MC becomes dominant. This regime is characterized by a partial conversion of the FW to the short wavelength modes, ion Bernstein wave (IBW) and ion cyclotron wave (ICW), at the MC layer [5]. The converted wave is commonly strongly absorbed by electrons within a narrow spatial region on much shorter time scale than the characteristic time for indirect bulk plasma heating via MH. Thus, as one of the methods to identify experimentally whether MH or MC heating occurs, is to study electron temperature response to ICRH power modulation [6, 7]. Beyond plasma heating itself, the MC regime has a number of promising applications in present-day and future fusion machines, e.g. driving non-inductive current and generating plasma rotation [8–13].

A number of experiments were performed at JET and ASDEX-U aimed at studying various ICRH heating schemes in H majority plasmas with helium-3 (^{3}He) minorities that can be used in the non-activated phase of ITER [14–18]. Both (^{3}He)–H schemes relevant for the half-field ($B_0 = 2.65\,{\rm T}$) and full-field ($B_0 = 5.3\,{\rm T}$) operation phase of ITER were tested recently. For the frequency range designed for the ITER ICRH

system ($f = 40 - 55$ MHz) two heating scenarios are feasible for the half-field H phase: fundamental IC heating of H majority ions at $f \approx 40$ MHz and second harmonic heating of ^{3}He minority ions at $f \approx 53$ MHz [18]. However, both of these scenarios have relatively low single-pass absorption with dominant fast wave electron heating. For the full-field H phase fundamental ion cyclotron heating of ^{3}He ions is the only scheme available for plasma heating, which commonly has an as good heating efficiency as any of fundamental minority ICRH scenarios. This scheme has been tested at JET [15, 16] by adopting the magnetic field ($B_0 \approx 3.6$ T) and ICRH frequency ($f \approx 37$ MHz) to locate ^{3}He cyclotron layer in the plasma center as it will be in ITER.

In JET experiments reported in Refs. [15, 16] (^{3}He)–H plasma heating was studied at very low ^{3}He concentrations. Mode conversion was found to be reached at ^{3}He concentrations $X[^3\text{He}] = n_{^3\text{He}}/n_e = 2 - 3\%$, which were substantially smaller than the values observed in (^{3}He)–D plasmas ($X[^3\text{He}] \approx 10 - 15\%$). Such a difference is explained by the fact that (^{3}He)–H is the so-called 'inverted' ICRH scenario. A key feature of the inverted scenarios is that the minority ion species have a smaller charge-to-mass ratio than the majority species, $(Z/A)_{\text{mino}} < (Z/A)_{\text{majo}}$. For these heating scenarios the MC layer is located between the ICRH antenna on the low-field side (LFS) and the minority cyclotron resonance (the FW encounters the MC layer first), while for standard scenarios – like in (^{3}He)–D plasmas – the minority cyclotron layer is located between the MC layer and the LFS antenna.

Those experiments highlighted an essential effect of impurities in the inverted (^{3}He)–H scenario. Three important issues due to plasma dilution with the carbon impurities were outlined (note that the experiments [15–18] were carried at JET with the inner vessel covered with carbon tiles). First, the heating region was found to be shifted appreciably away from where it was expected for pure plasma. Second, MC heating was complicated further through the appearance of the supplementary MC layer associated with carbon (C) impurities. The efficiency of ICRH heating in (^{3}He)–H JET plasmas with multiple MC layers was addressed in detail in Ref. [17] for the extended range of ^{3}He concentrations, showing in addition the complexity of the real time control of the minority level and, thus, difficulty in controlling the location of the MC layer in such plasmas. The third direct effect of carbon impurities on ICRH performance was the reduction of the transition ^{3}He minority concentration, $X_{\text{crit}}[^3\text{He}]$. Full-wave ICRH simulations have shown that for the plasma without the carbon the transition from MH to MC heating should occur at $X_{\text{crit}}[^3\text{He}] \approx 5\%$, while the experimentally observed levels at JET were lower [15].

Since August 2011 JET is operating with the new ITER-like wall, using beryllium (Be) and tungsten (W) as the new plasma facing materials. Therefore, it is instructive to assess and analyze the impact of modest amounts of first wall material impurities, which will enter the plasma due to the plasma-wall interaction, on the performance of ICRH heating. The aim of the present paper is to find a reasonable estimate for $X_{\text{crit}}[^3\text{He}]$ in (^{3}He)–H plasma, which corresponds to the change of the heating regime from MH to MC, and evaluate the effect of typical impurities at JET on that.

The paper is organized as follows. Section 2 shows 1D numerical results for the dependence of the transition ^{3}He concentration on the plasma and ICRH parameters in pure (^{3}He)–H plasma. We present two equivalent approaches for the analytical estimate of $X_{\mathrm{crit}}[^3\mathrm{He}]$ in section 3. In section 4 one of the approaches is generalized further to account for the impurities in the plasma. Also, the dependence of $X_{\mathrm{crit}}[^3\mathrm{He}]$ on the concentrations of Be and other impurities is analyzed there. Based on the results of previous sections, in section 5 we suggest a potential method to reduce and/or control $X_{\mathrm{crit}}[^3\mathrm{He}]$ by using additional puffing of ^{4}He ions to (^{3}He)–H plasma. Finally, conclusions are drawn in section 6.

2. Numerical results for the transition concentration of helium-3 ions in pure (^{3}He)–H plasma

To analyze the wave propagation and damping dynamics in the (^{3}He)–H plasma, the 1D ICRH full-wave code TOMCAT [19] has been used. This code solves a 12th order wave equation system, that guarantees a positive definite and purely resonant absorption for Maxwellian populations, accounting for the radial variation of the toroidal magnetic field and FW parallel wavenumber. It, however, omits the finite poloidal magnetic field effects, and thus excludes MC of the FW to the ICW. All the results reported assume pure excitation of the FW from the LFS of the tokamak as the imposed boundary conditions. TOMCAT gives scattering coefficients (reflection, transmission, conversion and absorption) for a single or a double transit of the FW over the plasma depending on a chosen radial range of integration. In contrast to usual full-wave codes, where all the RF power launched into the plasma is assumed to be absorbed (i.e. yielding multi-pass absorption), TOMCAT calculates the single- or double-pass absorption coefficients. The evaluation of a single- or a double-pass absorption coefficient allows for estimating the heating efficiency of the studied ICRH scenario qualitatively.

Even though TOMCAT can give only qualitative results (since many effects are not taken into account in a 1D geometry), it is helpful for understanding the global trends and some of the observed characteristics of the ICRH performance. TOMCAT simulations were used for the analysis of the past (^{3}He)–H experiments at JET and helped to identify the effect of C impurities in these scenarios [15, 17]. In a recent paper [20], the normalized absorption coefficients given by TOMCAT and the evaluated deuterium transition concentration in D-T plasma were found to be in a reasonable agreement with the results of more sophisticated modelling with the 2D full-wave code TORIC. We use therefore TOMCAT modelling to check and supplement the analytical estimates presented in this paper. However, it is important to note that a rigorous treatment of the FW propagation and MC in tokamaks should be essentially based on the 2D or 3D full-wave modelling [21–26].

Figure 1 shows the single-pass (left) and double-pass (right) absorption coefficients in (^{3}He)–H plasma, computed with TOMCAT. We consider plasma and ICRH parameters typical for past JET (^{3}He)–H experiments: plasma major and minor radius
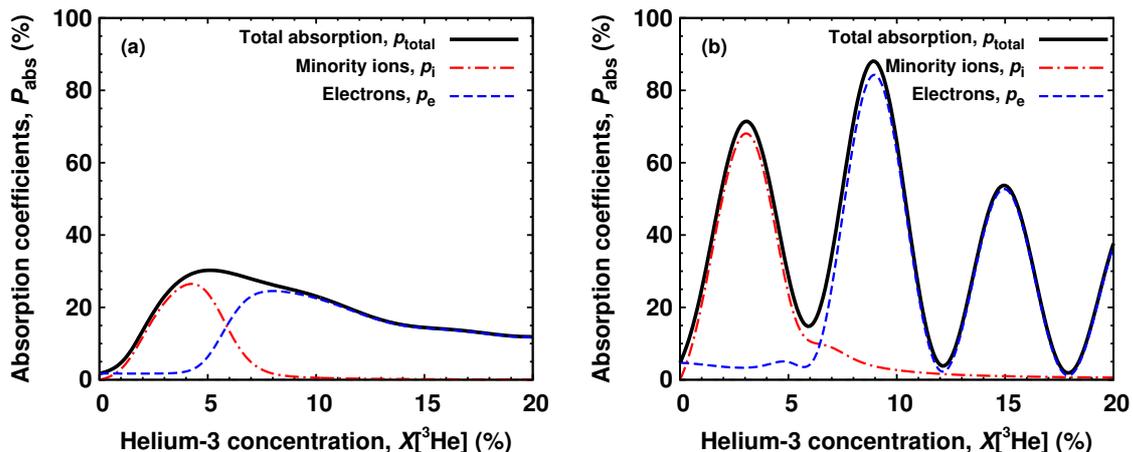
Figure 1. Single-pass (a) and double-pass (b) absorption coefficients vs. ^{3}He minority concentration calculated with the TOMCAT code for (^{3}He)–H plasma: $B_0 = 3.1$ T, $f = 32.2$ MHz, $n_{e0} = 3.2 \times 10^{19}$ m^{-3}, $T_0 = 5.0$ keV, $n_{\mathrm{tor}} = 27$.

$R_0 = 2.96$ m and $a = 0.9$ m, RF frequency $f = 32.2$ MHz, central magnetic field $B_0 = 3.1$ T, $n_e(r) = (n_{e0} - n_{e1})(1 - (r/a)^2) + n_{e1}$, central density $n_{e0} = 3.2 \times 10^{19}$ m^{-3}, edge density $n_{e1} = 0.1\, n_{e0}$, $T(r) = (T_0 - T_1)(1 - (r/a)^2)^{1.5} + T_1$, central electron and ion temperature $T_0 = 5.0$ keV, edge temperature $T_1 = 0.1\, T_0$, FW toroidal mode number is taken to be $n_{\mathrm{tor}} = 27$ ($k_{\parallel} = n_{\mathrm{tor}}/R$), typical for dipole phasing of the A2 ICRH antenna at JET. This choice of f and B_0 places ^{3}He cyclotron resonance almost centrally, $R_{^3\mathrm{He}} = 2.9$ m. The results we present in this section are computed assuming pure plasma without impurities.

For the considered parameters single-pass absorption by minority species reaches its maximum $p_i = 27.5\%$ at $X[^3\mathrm{He}] = 4.2\%$. Electron absorption at this minority concentration is only $p_e = 2.7\%$. Ion absorption starts to degrade with increasing $X[^3\mathrm{He}]$, whereas electron heating via mode conversion, in contrast, increases. At $X[^3\mathrm{He}] = 5.9\%$ minority ion heating is balanced by electron heating, and we refer to that $X[^3\mathrm{He}]$ as a transition concentration, and denote it with $X_{\mathrm{crit}}[^3\mathrm{He}]$. The maximum electron heating $p_e = 25.6\%$ is reached at $X[^3\mathrm{He}] = 8.1\%$, and starts to decrease for higher $X[^3\mathrm{He}]$ in agreement with the Budden theory for the isolated MC layer [27].

Figure 1(b) shows the absorption power fractions transferred in a double sweep of the FW in the plasma. The FW is followed from the incidence side (LFS) and is allowed to reflect once on the high-field side (HFS) cutoff. It exhibits oscillations in the double-pass absorption by electrons and significant increase in the absorption by ^{3}He ions in the MH regime. These are due to the multiple FW reflections in the plasma and constructive/destructive interference undergone by the reflected waves [20, 28–30]. Electron heating via mode conversion starts to dominate over minority ion heating at $X[^3\mathrm{He}] = 6.4\%$. The total phase difference, which defines the resulting double-pass absorption by ions and electrons, includes the terms due to the FW reflection on the minority cyclotron resonance and MC layer, respectively. In general, it is

different for minority and MC heating, and thus the discussed transition concentration $X_{\mathrm{crit}}[^3\mathrm{He}]$ differs somewhat from the value calculated for a single transit of the FW in the plasma. Since the FW interference complicates the analysis of the wave propagation and absorption, and the main emphasis of this paper is to sort out the effect of impurities on $X_{\mathrm{crit}}[^3\mathrm{He}]$, the numerical results presented in the paper rely on treating the propagation of the single incident wave and ignoring possible additional FW reflection from the HFS cutoff and supplementary MC layers (single-pass TOMCAT calculations) unless otherwise stated.

ICRH system on JET covers a frequency range from 23 to 57 MHz, providing access to a large number of scenarios for a wide range of magnetic fields [31]. In $(^3\mathrm{He})$–H ICRH experiments reported in [15, 17] different RF frequencies were used for plasma heating, $f \approx 37\,\mathrm{MHz}$ and $f \approx 32\,\mathrm{MHz}$, respectively. Figure 2(a) presents $X_{\mathrm{crit}}[^3\mathrm{He}]$ as a function of RF generator frequency f, but for the fixed f/B_0 ratio to keep the same location of the minority cyclotron resonance in the plasma, $R_{^3\mathrm{He}}$. The transition concentration $X_{\mathrm{crit}}[^3\mathrm{He}]$ decreases if operating at higher RF frequency and magnetic field: while for baseline case shown in Fig. 1 ($f/B_0 = 32.2/3.1$) transition from MH to MC was reached at $X[^3\mathrm{He}] = 5.9\%$, $X_{\mathrm{crit}}[^3\mathrm{He}]$ decreases to 5.1% if choosing $f/B_0 = 37.4/3.6$. $X_{\mathrm{crit}}[^3\mathrm{He}]$ follows approximately a $1/f$-dependence, which is clearly seen by comparing the numerical results with the fitting curve. It suggests that the transition concentration is connected to the Doppler width of the minority IC resonance, $\Delta R \propto \sqrt{2}k_\parallel v_{th,\mathrm{mino}}/\omega$, which is also inversely proportional to the RF frequency.

This interpretation is supported by Fig. 2(b), where the dependence of $X_{\mathrm{crit}}[^3\mathrm{He}]$ on the plasma temperature is depicted (all plasma species are assumed to have equal temperatures). The transition concentration of $^3\mathrm{He}$ ions raises with the temperature and scales as a square root of T_0. In future machines like ITER, where higher plasma temperatures are expected for the tokamak operation, the transition to MC in $(^3\mathrm{He})$–H plasmas is to occur at higher $^3\mathrm{He}$ concentrations than in JET. Figure 2(b) also shows that $X[^3\mathrm{He}]$, at which single-pass minority ion absorption is maximized (triangles), increases with T_0. Due to increased $^3\mathrm{He}$ demand and industrial consumption, the typical market price for $^3\mathrm{He}$ has raised from \$100 – \$200 per liter to \$2,000 per liter in recent years [32]. Along with the fact that the plasma volume in ITER is almost 10 times larger than in JET, this increases significantly the operational costs for using $^3\mathrm{He}$ in future fusion devices. The present paper discusses the possibility to retune ICRH scenarios involving helium-3 ions to minimize $^3\mathrm{He}$ concentrations needed for MH and MC heating.

As follows from Fig. 2(c), the transition concentration increases with the FW toroidal wavenumber, which is consistent with the increase in the Doppler broadening of the cyclotron resonance for higher $k_\parallel$. However, the calculated values of $X_{\mathrm{crit}}[^3\mathrm{He}]$ are less sensitive to the value of n_{tor} than the estimates yielded from the linear fitting. A moderate increase in $X_{\mathrm{crit}}[^3\mathrm{He}]$ is also observed if increasing the central plasma density, as Fig. 2(d) illustrates. The reason why $X_{\mathrm{crit}}[^3\mathrm{He}]$ raises with n_{e0} will be outlined in the next section, where we present simplified analytical models that help us to grasp the main physical parameters affecting $X_{\mathrm{crit}}[^3\mathrm{He}]$.
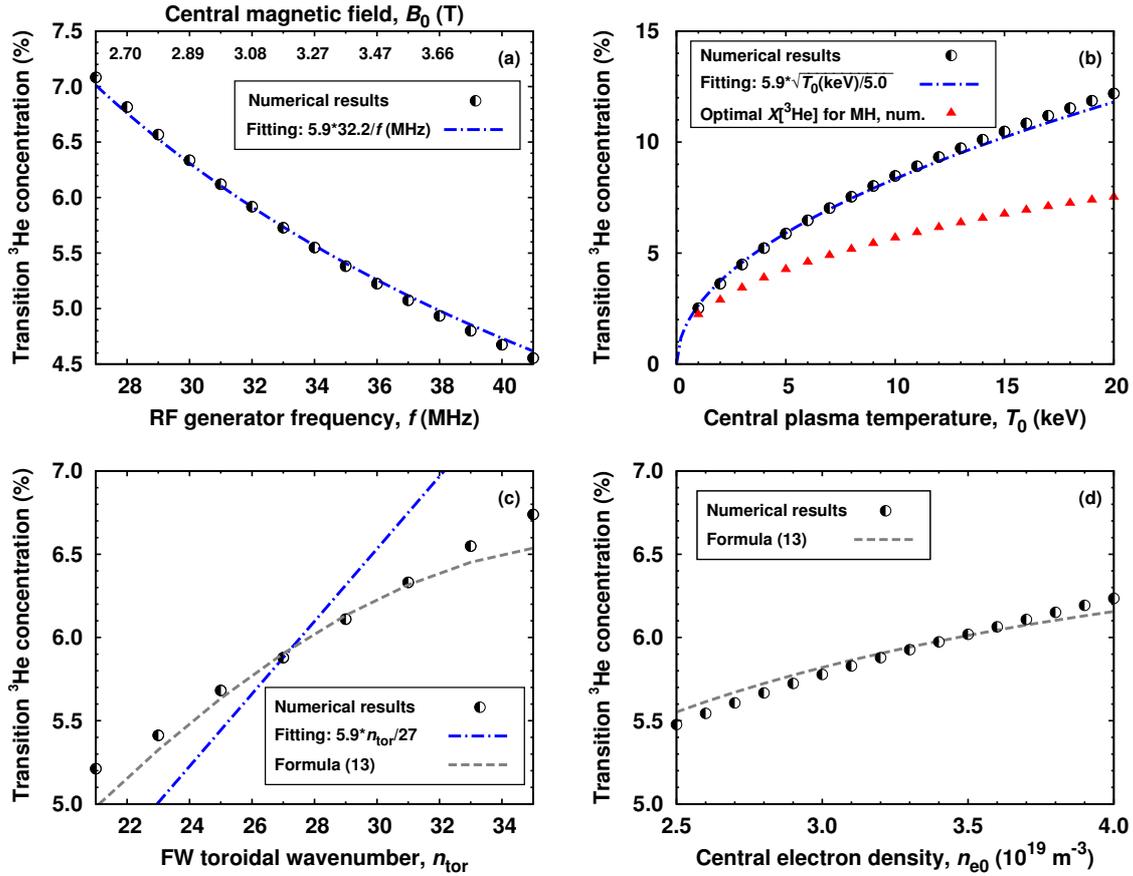
Figure 2. Transition concentration of ^{3}He ions as a function of RF frequency (f/B_0 fixed) (a), central plasma temperature (b), FW toroidal wavenumber (c) and central plasma density (d).

3. Analytical estimates for the transition concentration of helium-3 ions in pure (^{3}He)–H plasma

ICRH heating of fusion plasmas relies on the transport of the energy by the fast waves from the edge of the plasma to the core. The FW propagating at the equatorial plane of a tokamak is fairly well described by the dispersion relation

$$n_{\perp,\mathrm{FW}}^2 = \frac{(\epsilon_\mathrm{L} - n_\parallel^2)(\epsilon_\mathrm{R} - n_\parallel^2)}{\epsilon_\mathrm{S} - n_\parallel^2}, \tag{1}$$

where $n_\parallel = ck_\parallel/(2\pi f)$ is the refractive index parallel to the equilibrium magnetic field, and f is the RF generator (antenna) frequency. Omitting the poloidal magnetic field, the FW parallel wavenumber varies radially as $k_\parallel = n_{\mathrm{tor}}/R$; the dominant n_{tor} in the launched FW spectrum is determined by the antenna geometry and chosen antenna phasing. In Eq. (1), ϵ_S, ϵ_L and ϵ_R are the plasma dielectric tensor components in the notation of Stix [4], which in a cold-plasma limit and for the ICRH frequency range are

given by

$$\epsilon_S \approx 1 + \frac{\omega_{pe}^2}{\omega_{ce}^2} - \sum_i \frac{\omega_{pi}^2}{\omega^2 - \omega_{ci}^2},$$

$$\epsilon_L \approx 1 + \frac{\omega_{pe}^2}{\omega_{ce}^2} + \sum_i \frac{\omega_{pi}^2}{\omega_{ci}(\omega_{ci} - \omega)}, \qquad (2)$$

$$\epsilon_R \approx 1 + \frac{\omega_{pe}^2}{\omega_{ce}^2} + \sum_i \frac{\omega_{pi}^2}{\omega_{ci}(\omega_{ci} + \omega)},$$

where the summation is to be taken over all ion species constituting the plasma, and ω_{ps} and ω_{cs} are the species' plasma and cyclotron frequencies, respectively.

The FW resonance condition $\epsilon_S = n_\parallel^2$ defines the location of the MC layer, often called also as the ion-ion hybrid (IIH) resonance. Hot plasma theory resolves this resonance and bends it into a confluence. At this layer the FW is converted partially to a short wavelength mode, the IBW and the ICW, depending on the relation between the plasma temperature and poloidal magnetic field. The MC layer is accompanied closely to the LFS by the left-hand polarized cutoff (L-cutoff) defined by the condition $\epsilon_L = n_\parallel^2$. In Appendix A of the paper we present the derivation of the formulas for resonant frequencies, ω_S and ω_L, satisfying the conditions

$$\epsilon_S = n_\parallel^2,$$
$$\epsilon_L = n_\parallel^2, \qquad (3)$$

which we refer to further as the IIH and L-cutoff frequencies, respectively.

Since the toroidal magnetic field follows $1/R$ dependence in tokamaks, the location of the layer, at which the antenna frequency ω matches a certain resonant frequency ω_i ($\omega = 2\pi f = \omega_i$), can be calculated as follows

$$R|_{\omega=\omega_i} = R_0 \frac{\omega_i}{\omega_{cH}} \frac{15.25\, B_0(\mathrm{T})}{f(\mathrm{MHz})}, \qquad (4)$$

where ω_{cH} is the cyclotron frequency for hydrogen ions. As an example, for the baseline conditions chosen ($f = 32.2\,\mathrm{MHz}$, $B_0 = 3.1\,\mathrm{T}$) the hydrogen IC resonance is located at $R_H = 4.34\,\mathrm{m}$, ^{3}He resonance – at $R_{^3\mathrm{He}} = 2.90\,\mathrm{m}$, Be resonance – at $R_{\mathrm{Be}} = 1.93\,\mathrm{m}$. Vice versa, using Eq. (4) we can connect the radial coordinate in the plasma, R_i to the corresponding resonant frequency, ω_i.

For the discussion of the transition minority concentration and in order to understand how two ICRF heating regimes arise in two-ion component plasmas, we need to account for the kinetic response of the resonant minority ions in the ϵ_S tensor component in the denominator of Eq. (1) [3]. To keep the algebra simpler, we consider the leading order terms in finite Larmor radius expansion of ϵ_S. Then, it can be written as follows

$$\epsilon_S = 1 + \frac{\omega_{pe}^2}{\omega_{ce}^2} + \sum_{i=1,2} \frac{\omega_{pi}^2}{2\omega^2} \frac{\omega}{\sqrt{2}k_\parallel v_{ti}} \left[Z(\xi_{1i}) + Z(\xi_{-1i}) \right], \qquad (5)$$

where $Z(\xi)$ is the plasma dispersion function, $v_{ti} = (T_i/m_i)^{1/2}$ is the thermal velocity, and $\xi_{\pm 1i} = (\omega \pm \omega_{ci})/(\sqrt{2}k_\parallel v_{ti})$. Following Ref. [3], throughout the paper indices '1' and

'2' refer to majority (hydrogen) and minority (helium-3) ions, respectively. Majority species are non-resonant, so one could use asymptotic expansion of the plasma dispersion function for large arguments, $Z(\xi) \simeq -1/\xi$. For minority ions the term proportional to $Z(\xi_{12})$ is non-resonant, while the term proportional to $Z(\xi_{-12})$ represents resonant minority response. In such a way, we could write ϵ_S tensor element as

$$\epsilon_S \approx -\frac{\omega_{p1}^2}{\omega^2 - \omega_{c1}^2} - \frac{\omega_{p2}^2}{2\omega(\omega + \omega_{c2})} + \frac{\omega_{p2}^2}{2\omega^2}\frac{\omega}{\sqrt{2}k_\parallel v_{t2}}Z(\xi_{-12}). \tag{6}$$

Accounting for $\omega \approx \omega_{c2}$ and that the minority concentration is typically much lower than that of majority level, the resonance condition $\epsilon_S = n_\parallel^2$ can be re-written

$$Z(\xi_{-12}) = \frac{2\omega_{p1}^2}{\omega_{p2}^2}\frac{\sqrt{2}k_\parallel v_{t2}}{\omega}\left[\frac{\mu^2}{1-\mu^2} + \frac{k_\parallel^2 v_{A1}^2}{\omega^2}\right], \tag{7}$$

where we have introduced $\mu = Z_1 A_2 / Z_2 A_1$, and v_{A1} is the Alfvén speed corresponding to the majority ions. The real part of $Z(\xi)$ function is shown in Fig. 3; note that the argument of the plasma dispersion function is proportional to the distance from the minority cyclotron resonance layer ($R_2 = R_0 + x_2$)

$$\xi_{-12}(x) = \frac{\omega}{\sqrt{2}k_\parallel v_{t2}}\frac{x - x_2}{R_2}. \tag{8}$$

The right-hand side of Eq. (7) depends on the minority concentration $X_2 = n_2/n_e$ via ω_{p2}^2 in the denominator, but is independent of ξ_{-12} and thus is represented by a horizontal line in Fig. 3. Note that the second term in Eq. (7) is small compared to the first for the typical experimental conditions. The resonance and MC occur provided there is an intersection of the horizontal line with the curve for $Z(\xi)$ function. For the standard ICRH scenarios $\mu < 1$, while for the inverted $-\mu > 1$; therefore, the resonance condition for MC can be fulfilled only on the HFS and LFS of the minority IC resonance, respectively.

In Fig. 3 we have depicted 4 horizontal lines corresponding to different minority concentrations. When X_2 is very small, there is no intersection of the horizontal line (dotted) with $\mathrm{Re}[Z(\xi)]$ and thus the resonance condition for MC does not occur. The FW is absorbed by minority ions due to the imaginary part of $Z(\xi_{-12})$ and gives rise to the MH regime. When, on the contrary, X_2 is very high, there is always an intersection at $|\xi_{-12}| > 5$, for which the imaginary part of $Z(\xi)$ is negligible (dashed line). This is a MC regime, when the absorption is defined by the local resonance and there is almost no minority damping. When the minority concentration is such that the horizontal curve is tangential to the real part of $Z(\xi)$, then MC starts to occur (dash-dotted line). Since the maximum absolute value of $\mathrm{Re}[Z(\xi)]$ is approximately unity, then we can derive the corresponding minority concentration to be [3]

$$X_2^{(\text{Wesson})} = \frac{\sqrt{2}k_\parallel v_{t2}}{\omega}\frac{2A_1}{A_2 Z_1}\left[\frac{\mu^2}{|1-\mu^2|} \pm \frac{k_\parallel^2 v_{A1}^2}{\omega^2}\right]. \tag{9}$$

The difference between Eq. (9) and the result presented in Ref. [3] is '$\pm$' sign for the second term: plus/minus sign should be taken for the standard/inverted ICRH scenario,
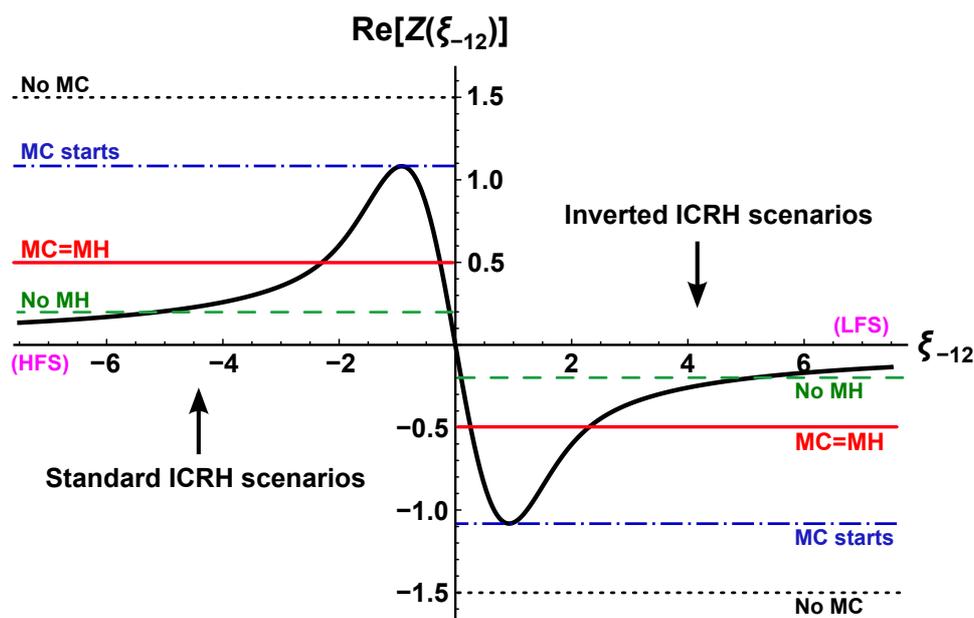
Figure 3. MC occurs when there is an intersection of the horizontal line, which represents the right-hand side of Eq. (7), with the real part of the plasma dispersion function, $Z(\xi_{-12})$. For the standard/inverted ICRH scenarios the resonance condition $\epsilon_{\mathrm{S}} = n_{\parallel}^2$ is fulfilled to the HFS/LFS of the minority IC layer, respectively.

respectively. The physical interpretation for this fact is given in the Appendix B of the paper. Since $v_{A1}^2 \propto 1/n_e$, for the inverted (^{3}He)–H scenario the transition minority concentration slightly increases with the plasma density as it was shown in Fig. 2(d). Note that criterion expressed by Eq. (9) was first indicated by Takahashi [33]. In Ref. [34], Lashmore-Davies *et al* generalized this expression for the cases of degenerate resonances in (H)–D plasmas (the majority second harmonics coincides with the minority fundamental) and a single-species second harmonic heating.

We can obtain the same result as that given by Eq. (9) using the different approach. Apart from giving additional physical insight, this approach will make it easier to include the effect of multiple impurities in the model. Qualitatively the transition from the minority heating to mode conversion heating can be explained as follows (see Fig. 4). Minority cyclotron resonance has a finite Doppler width, $\Delta R = p_0 \sqrt{2} k_{\parallel} v_{t2} R/\omega$, where the numerical coefficient p_0 is of the order of unity. Let denote δ as a distance between the cold-plasma IIH resonance and the minority IC layer. For small minority concentrations the IIH layer is located within the Doppler broadened IC resonance (shaded area in Fig. 4), and minority heating dominates (Fig. 4(a)). For large minority concentrations the IIH resonance is located out of the region, where the cyclotron damping by minority ions is important, such that $\delta > \Delta R$, and electron heating via mode conversion will become the main absorption mechanism (Fig. 4(b)). As noted in Ref. [12], the transition from MH to MC is reached when $\delta = \Delta R$, i.e. when the mode conversion layer passes through the broadened IC resonance.
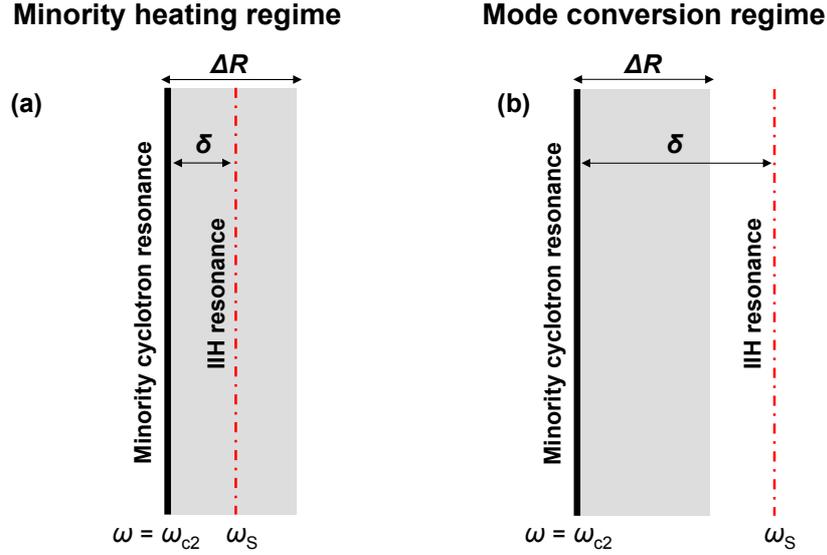
Figure 4. Transition from MH (a) to MC (b) heating regime occurs when the IIH resonance passes through the Doppler broadened minority cyclotron layer (the scheme corresponds to the inverted ICRH scenario, for which the IIH resonance is to the LFS of the minority IC layer).

For the tangential case discussed in Ref. [3], the intersection of the curves occurs at $|\xi_{-12}| \approx 1$. At this minority concentration, MC only starts to occur and is much weaker than minority ion damping. MC is expected to have the same absorption strength as the ion absorption for higher X_2, when $|\text{Re}[Z(\xi_{-12})]| \simeq 0.5$ (solid line in Fig. 3). The argument of the plasma dispersion function, which is formally the constant p_0 (cf. Eq. (8)), for this case equals to $\xi_{-12} \simeq \pm 2.3$. According to Eq. (4), the radial coordinate $R_2 \pm \Delta R$ corresponds to the normalized frequency ($\tilde{\omega} = \omega/\omega_{cH}$)

$$\tilde{\omega}_\Delta = \mathcal{Z}_2 \left[1 \pm p_0 \sqrt{2} k_\parallel v_{t2}/\omega \right], \tag{10}$$

where $\mathcal{Z}_i = Z_i/A_i$ denotes the ratio of the charge number to the atomic mass for ion species.

At the same time the normalized IIH frequency (satisfying the condition $\epsilon_S = n_\parallel^2$) as a function of the minority concentration and $k_\parallel$ is given by (see Appendix A)

$$\tilde{\omega}_S \approx \mathcal{Z}_2 + \frac{\mathcal{Z}_1^2 - \mathcal{Z}_2^2}{2\mathcal{Z}_1} f_2 + \frac{(\mathcal{Z}_1^2 - \mathcal{Z}_2^2)^2}{2\mathcal{Z}_1^2} \alpha f_2, \tag{11}$$

where we introduced the convenient notation $f_i = Z_i X_i$ for the fraction of electrons replaced by the ion species 'i'. The last term in Eq. (11) describes the shift of the IIH resonance due to finite n_{tor}, $\alpha = (\omega_{cH}^2/\omega_{pH}^2) n_\parallel^2$, $\omega_{pH}^2 = 4\pi n_e e^2/m_H$. The condition $\delta = \Delta R$ (corresponding to $\tilde{\omega}_\Delta = \tilde{\omega}_S$) will be fulfilled if

$$X_{2,\text{crit}} = p_0 \frac{\sqrt{2} k_\parallel v_{t2}}{\omega} \frac{2}{A_2} \left[\frac{\mathcal{Z}_1}{|\mathcal{Z}_1^2 - \mathcal{Z}_2^2|} \pm \alpha \right], \tag{12}$$

which is the same as $X_2^{\text{(Wesson)}}$ given in Eq. (9) (except the multiplier p_0), but written with the new notation ($\alpha \mathcal{Z}_1 = k_\parallel^2 v_{A1}^2 / \omega^2$). For the tangential case, which corresponds to the beginning of MC, $p_0 \approx 1$ and the results given by Eqs. (9) and (12) are identical. On the other hand, to estimate the transition minority concentration $p_0 \approx 2.3$ should be used, yielding for (^{3}He)–H plasma ($\mathcal{Z}_1 = 1$, $\mathcal{Z}_2 = 2/3$)

$$X_{\text{crit}}[^3\text{He}] \approx 2.3 \frac{\sqrt{2}k_\parallel v_{t2}}{\omega}(1.2 - 2\alpha/3). \tag{13}$$

An additional argument for choosing the horizontal intersection level with $\text{Re}[Z(\xi)]$ curve in Fig. 3 to be lower than unity is due to the good correspondence between the numerical results and the analytical formula (13) which is presented in Figs. 2(c) and (d).

In this section we considered pure two-ion majority/minority plasma excluding the presence of impurities. The critical minority concentration in diluted plasmas will be upshifted or downshifted $\tilde{X}_{2,\text{crit}} = M_{\text{imp}}X_{2,\text{crit}}$, if accounting for impurities that provide the correction factor M_{imp}. Thus, the choice of p_0 constant affects the absolute value for the transition concentration, but it is actually not important to describe the relative influence of impurities on that, which is a subject of the next chapter.

4. Transition concentration of helium-3 ions in (^{3}He)–H plasma accounting for impurities

The reason why impurities affect the transition concentration of minority ions can easily be understood by noting that the location of the IIH resonance depends on the level of impurity contamination. In pure plasma it is described by Eq. (11), but as impurities are accounted for additional terms arise. In Ref. [30], three-ion component plasmas were considered, and the correction term describing the effect of a single impurity species was obtained. In Appendix A of this paper, we generalize those formulas to take into account any number of impurity species. It is shown, that to the lowest order the contribution to $\tilde{\omega}_{\text{S}}$ caused by impurities is described by the expression

$$\delta\tilde{\omega}_{\text{S}} \approx \sum_{\text{imp}} \frac{(\mathcal{Z}_1 + \mathcal{Z}_2)(\mathcal{Z}_2^2 + \mathcal{Z}_1\mathcal{Z}_{\text{imp}})}{2\mathcal{Z}_1^2(\mathcal{Z}_2 + \mathcal{Z}_{\text{imp}})} \frac{(\mathcal{Z}_1 - \mathcal{Z}_2)(\mathcal{Z}_1 - \mathcal{Z}_{\text{imp}})}{(\mathcal{Z}_2 - \mathcal{Z}_{\text{imp}})} f_2 f_{\text{imp}}. \tag{14}$$

Note that in the corresponding formula, derived for a single impurity in Ref. [30], due to a misprint a $1/(2\mathcal{Z}_2)$ factor is missing in a term describing the impurity response. If we denote $X_{2,\text{crit}}$ to be the transition minority concentration in a pure plasma, and $\tilde{X}_{2,\text{crit}}$ as that in plasmas with impurities, then the following approximate formula can be obtained

$$\tilde{\omega}_{\text{S}} \approx \mathcal{Z}_2 + \frac{\mathcal{Z}_1^2 - \mathcal{Z}_2^2}{2\mathcal{Z}_1}f_2 + \frac{(\mathcal{Z}_1^2 - \mathcal{Z}_2^2)^2}{2\mathcal{Z}_1^2}\alpha f_2 \approx \mathcal{Z}_2 + \frac{\mathcal{Z}_1^2 - \mathcal{Z}_2^2}{2\mathcal{Z}_1}\tilde{f}_2 +$$
$$+ \frac{(\mathcal{Z}_1^2 - \mathcal{Z}_2^2)^2}{2\mathcal{Z}_1^2}\alpha\tilde{f}_2 + \sum_{\text{imp}} \frac{(\mathcal{Z}_1^2 - \mathcal{Z}_2^2)(\mathcal{Z}_2^2 + \mathcal{Z}_1\mathcal{Z}_{\text{imp}})(\mathcal{Z}_1 - \mathcal{Z}_{\text{imp}})}{2\mathcal{Z}_1^2(\mathcal{Z}_2^2 - \mathcal{Z}_{\text{imp}}^2)}\tilde{f}_2 f_{\text{imp}}. \tag{15}$$

From Eq. (15) it is easy to show that

$$\tilde{f}_2/f_2 \approx 1 - \sum_{\text{imp}} \frac{(\mathcal{Z}_1 - \mathcal{Z}_{\text{imp}})(\mathcal{Z}_2^2 + \mathcal{Z}_1\mathcal{Z}_{\text{imp}})}{(1 + \alpha(\mathcal{Z}_1^2 - \mathcal{Z}_2^2)/\mathcal{Z}_1)\mathcal{Z}_1(\mathcal{Z}_2^2 - \mathcal{Z}_{\text{imp}}^2)}f_{\text{imp}}. \tag{16}$$

Table 1. Rough estimates for the impurity concentrations at JET equipped with the new ITER-like wall.

	Be^{4+}	C^{6+}	W^{46+}	Ni^{26+}
X_{imp}	2.5×10^{-2}	1.5×10^{-3}	1.0×10^{-4}	1.0×10^{-4}
f_{imp}	0.10	0.009	0.005	0.003
ΔZ_{eff}	0.30	0.05	0.21	0.07

In the denominator of Eq. (16), $\alpha(\mathcal{Z}_1^2 - \mathcal{Z}_2^2)/\mathcal{Z}_1$ can be neglected since accounting for that gives the contribution $\propto \alpha f_{imp}$, and a number of quadratic terms have already been omitted when deriving Eq. (14). These quadratic terms are summarized in the Appendix A of the paper. Thus, the transition minority concentrations in pure and plasmas contaminated with impurities are related as follows

$$\frac{\tilde{X}_{2,crit}}{X_{2,crit}} \approx 1 - \sum_{imp} \frac{(\mathcal{Z}_1 - \mathcal{Z}_{imp})(\mathcal{Z}_2^2 + \mathcal{Z}_1 \mathcal{Z}_{imp})}{\mathcal{Z}_1(\mathcal{Z}_2^2 - \mathcal{Z}_{imp}^2)} f_{imp}. \qquad (17)$$

Since in (^{3}He)–H plasmas $\mathcal{Z}_1 > \mathcal{Z}_2 > \mathcal{Z}_{imp}$, the impurity contamination leads to the reduction of the transition concentration of helium-3 ions ($M_{imp} < 1$):

$$M_{imp} = \frac{\tilde{X}_{crit}[^3He]}{X_{crit}[^3He]} \approx 1 - 8X[Be] - 14.6X[C^{6+}] - 33.6X[W^{28+}] - $$
$$-62.7X[W^{46+}] - 51.4X[Ni^{26+}] - ... \qquad (18)$$

Estimates for the concentrations of impurities typical at JET are summarized in Table 1. The data has been taken from Refs. [35–37]. Similarly to the effect of C ions for the old JET wall, the presence of Be is expected to be the main contributing impurity to the reduction factor M_{imp} for the new ITER-like wall.
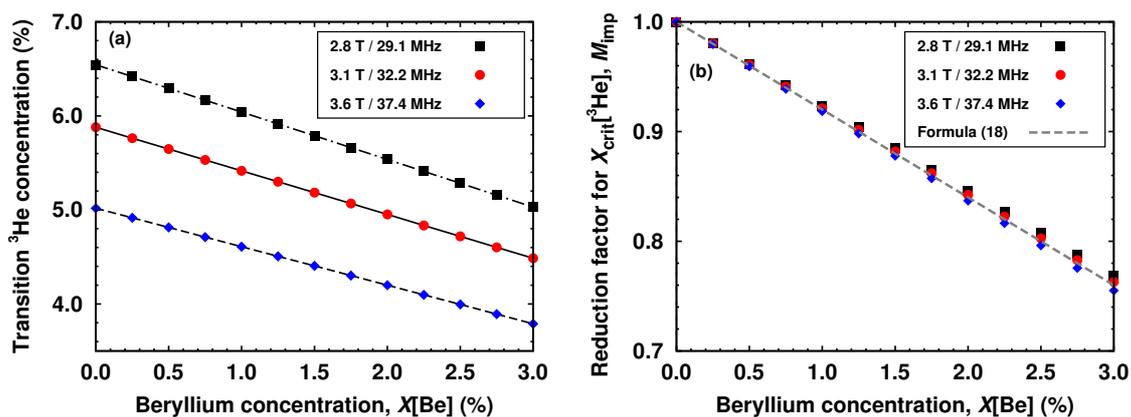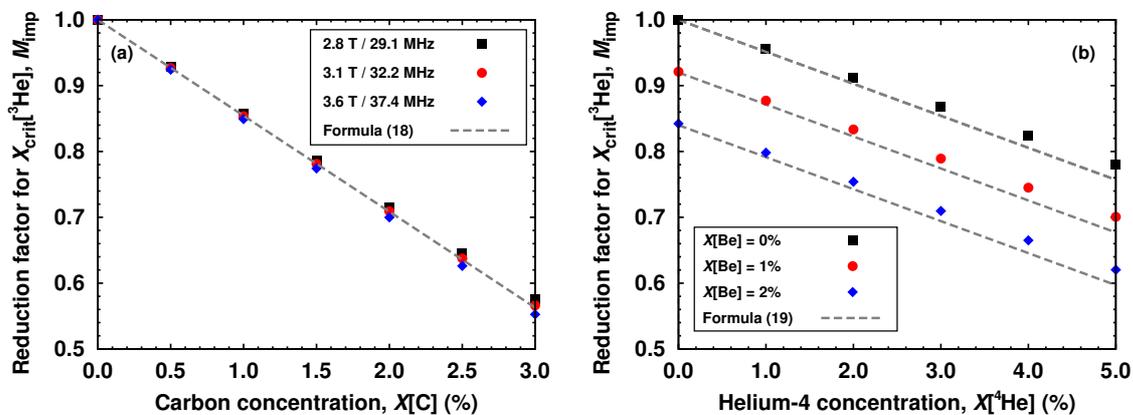

Figure 5. (a) Transition concentration of helium-3 ions in (^{3}He)–H plasma as a function of $X[Be]$ for different f and B_0. (b) Relative change of $X_{crit}[^3He]$ is independent of f and decreases almost linearly with beryllium concentration.

Although a number of simplified assumptions have been made to derive Eq. (18), it gives a remarkably good correspondence with numerical values. Figure 5(a) shows

the transition concentration of ^{3}He ions as a function of Be concentration for different f and B_0 (f/B_0 fixed), calculated numerically with the TOMCAT solver. As discussed, $X_{\text{crit}}[^3\text{He}]$ is smaller if operating at higher antenna frequencies. Regardless which RF frequency f is chosen, the transition concentration decreases with the concentration of Be impurities. As shown in Fig. 5(b), the relative change of $X_{\text{crit}}[^3\text{He}]$ due to the presence of Be does not depend on f and is in a very good correspondence with Eq. (18), $M_{\text{imp}} = 1 - 8X[\text{Be}]$.

The numerical factors, which appear in Eq. (18), have been tested for other impurities, and Fig. 6(a) shows an excellent agreement for C ions (relevant for the old JET wall). The values in Fig. 6 are calculated numerically with the TOMCAT solver. A rough estimate for Be concentration at JET, $X[\text{Be}] = 2.5\%$ ($\Delta Z_{\text{eff}} = 0.3$), should result in the reduction of the transition concentration of helium-3 ions by about 20%; it is smaller than the effect of carbon impurities reported previously ($X[\text{C}^{6+}] = 2.5\%$ corresponds to $\Delta Z_{\text{eff}} = 0.75$ and $M_{\text{imp}} = 0.63$). Accounting for another impurities present in the plasma leads to a small further decrease of M_{imp}, $M_{\text{imp}} \approx 0.75$. Thus, for similar experimental conditions the transition from MH to MC is expected to occur at somewhat higher ^{3}He concentrations for the new JET wall in comparison with those reported for the old carbon wall. Along with the approximate formula (13), Eq. (18) can serve as a rough estimate for the transition concentration of helium-3 ions in (^{3}He)–H plasmas for JET-like plasmas.

Figure 6. Transition concentration of helium-3 ions in (^{3}He)–H plasma as a function of carbon (a) and helium-4 (b) concentrations. Figure (b) is for $f = 32.2\,\text{MHz}$ and $B_0 = 3.1\,\text{T}$.

5. Suggestion for puffing ^{4}He ions to (^{3}He)–H plasma to control transition from MH to MC regime

In view of the temperature dependence of $X_{\text{crit}}[^3\text{He}]$ shown in Fig. 2(b) and the arguments concerning the price of $X[^3\text{He}]$, using smaller helium-3 concentrations for running (^{3}He)–H experiments is beneficial. Depending on the specific goals envisaged for

the ICRH system one might need to set the experimental conditions to reach either MH ($X[^3\text{He}] < X_\text{crit}[^3\text{He}]$) or MC heating ($X[^3\text{He}] > X_\text{crit}[^3\text{He}]$): operating in MH regime is preferred to increase the fraction of thermal ion heating in (^{3}He)–H plasmas, whereas MC could be potentially used for driving the current or local plasma control. Therefore, the development of the methods to decrease and possibly control the minority concentrations needed for efficient ICRH performance is of high importance. As discussed in the previous section of the paper, plasma dilution with impurities leads to the reduction of $X[^3\text{He}]$, at which the transition from minority heating to mode conversion occurs. This section discusses briefly the possibility of $X_\text{crit}[^3\text{He}]$ reduction by puffing additional gas to (^{3}He)–H mixture.

The concentration of intrinsic Be impurities in a plasma is determined mostly by the level of plasma-wall interaction. It cannot be changed in a wide range and within a short time period that is a prerequisite to control the transition concentration of minority ions. However, additional puffing of ^{4}He ions to (^{3}He)–H plasma seems to potentially fulfil this goal. ^{4}He is a D-like species, and its price is much lower than the price for helium-3. As follows from Eq. (18), we expect that $X_\text{crit}[^3\text{He}]$ decreases with the concentration of helium-4 ions according to

$$M_\text{imp} \approx 1 - 8X[\text{Be}] - 4.9\text{X}[^4\text{He}]. \tag{19}$$

Figure 6(b) shows the comparison of the results given by Eq. (19) and the values calculated numerically with the TOMCAT solver for the baseline parameters considered ($f = 32.2\,\text{MHz}$ and $B_0 = 3.1\,\text{T}$). In plasmas without Be ions, addition of 5% and 10% of helium-4 ions to the (^{3}He)–H plasma decreases the transition concentration $X_\text{crit}[^3\text{He}]$ by 22% and 44%, respectively. Accounting for the presence of Be ions in the plasma, even smaller fractions of helium-4 can be used for minority ion control. As Fig. 7 illustrates, for plasmas including Be impurities at the level of 2%, by puffing 7% of ^{4}He one obtains similar transition concentration $X_\text{crit}[^3\text{He}]$ as those in pure (^{3}He)–H plasmas with $X[^4\text{He}] = 10\%$ puffing.

If a fraction of fuel hydrogen ions are replaced by ^{4}He ions the effective charge Z_eff will raise. But at the same time the level of ^{3}He, which also contributes to Z_eff, decreases, so the resulting increase of the effective charge is reasonably small, $\Delta Z_\text{eff} \approx 0.1 - 0.15$. Therefore it seems to be worth exploring this option in detail in separate studies.

A similar potential method to control $X_\text{crit}[^3\text{He}]$ could be applied if operating with deuterium majority plasmas, in which helium-3 is partially burn down via the fusion reaction $\text{D} + {}^3\text{He} \rightarrow {}^4\text{He}(3.6\,\text{MeV}) + p(14.7\,\text{MeV})$. By adding $X[\text{H}] = 15\%$ to (^{3}He)–D plasmas, the transition concentration of helium-3 ions in such plasmas can be reduced by a factor of $\sim 0.75 - 0.8$.

6. Conclusions

ITER will start its operation using the hydrogen majority plasmas to minimize the activation of the tokamak components. Since the access to H-mode in that plasmas will
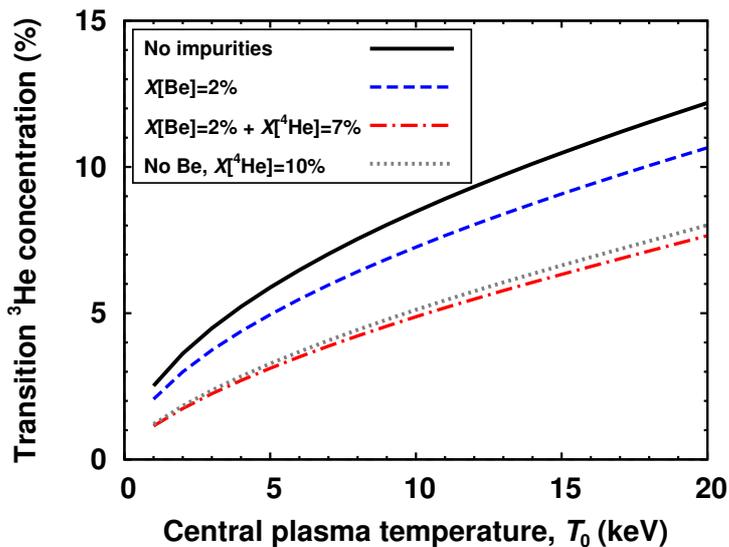
Figure 7. Transition concentration of helium-3 ions in (^{3}He)–H plasma increases with raising the plasma temperature. By puffing ^{4}He ions, $X_{\mathrm{crit}}[^3\mathrm{He}]$ can potentially be reduced and/or controlled.

not be assured with the available heating powers, it is of high importance to maximize the heating performance for the non-activated phase of ITER operation. ICRH is one of the heating systems to be used in ITER, and a number of ICRH experiments were performed at JET to develop and optimize heating scenarios relevant for such plasmas. One of the promising ICRH schemes relies on the use of the resonant minority ^{3}He ions to absorb the RF energy.

Past JET experiments with the old wall consisting of carbon tiles highlighted a number of specific features when applying ICRH in (^{3}He)–H plasmas. Particularly, a significant effect of intrinsic carbon impurities was revealed in that experiments. The heating region was found to be shifted radially comparing to the heating maximum expected in a pure plasma, and that was attributed to the presence of impurities. Under certain conditions C impurities also produced a supplementary MC layer, and multiple MC dynamics was observed in (^{3}He)–H plasmas. In addition, the concentration of minority ^{3}He ions, at which the transition from MH to MC occurs, was reported to be lower than that predicted by numerical simulations if the effect of impurities was neglected.

In the present paper we discuss how the transition concentration of ^{3}He ions depends on the plasma and ICRH parameters. It is shown that $X_{\mathrm{crit}}[^3\mathrm{He}]$ is related to the Doppler broadening of the minority IC layer, and thus is inversely proportional to the antenna frequency and increases with the plasma temperature and FW toroidal wavenumber. Using two equivalent analytical approaches, we generalize the formula for the transition minority concentration given in Ref. [3] for the case of inverted ICRH scenarios, which (^{3}He)–H scheme belongs to. This allows us to explain a small increase of $X_{\mathrm{crit}}[^3\mathrm{He}]$ with the plasma density in (^{3}He)–H plasmas.

Accounting for multiple impurity species always present in the plasma, we show that $X_{\mathrm{crit}}[^3\mathrm{He}]$ decreases and scales almost linearly with the impurity concentrations. An analytical estimate for the relative change of $X_{\mathrm{crit}}[^3\mathrm{He}]$ due to impurities is derived, and is shown to be in a good correspondence with the numerical results. We demonstrate that Be is to be the main impurity species affecting $X_{\mathrm{crit}}[^3\mathrm{He}]$ in $(^3\mathrm{He})$–H plasmas for JET equipped with the new ITER-like wall. A reduction of $X_{\mathrm{crit}}[^3\mathrm{He}]$ by $\sim 20-25\%$ is predicted if considering typical Be and another impurity concentrations at JET. A possible method to reduce and control $^3\mathrm{He}$ level, at which the transition from MH to MC is to occur, is suggested: the method relies on the additional puffing of $^4\mathrm{He}$ ions to $(^3\mathrm{He})$–H plasmas. We show that for $X[^4\mathrm{He}] = 5-10\%$ the reduction of the transition concentration of helium-3 ions by a factor of ~ 0.6 can be expected.

Since a number of simplifying assumptions have been made in this paper, the results can serve only as a qualitative estimates rather quantitative predictions. However, our results support the earlier experimental findings and allows to understand the basics of the underlined ICRH physics and interpolate the discussed effect accounting for new impurity species present in a plasma. Further numerical modelling and experimental support is needed to confirm the potential of using $^4\mathrm{He}$ gas puffing for $X_{\mathrm{crit}}[^3\mathrm{He}]$ control in $(^3\mathrm{He})$–H plasmas.

7. Acknowledgements

Appendix A. IIH and L-cutoff frequencies accounting for multiple impurity species and $n_{\mathrm{tor}} \neq 0$

In the IC frequency range the cold plasma tensor components are given by

$$
\begin{aligned}
\epsilon_{\mathrm{S}} &= 1 + \frac{\omega_{pe}^2}{\omega_{ce}^2} - \sum_i \frac{\omega_{pi}^2}{\omega^2 - \omega_{ci}^2}, \\
\epsilon_{\mathrm{L}} &= 1 + \frac{\omega_{pe}^2}{\omega_{ce}^2} - \sum_i \frac{\omega_{pi}^2}{\omega_{ci}(\omega - \omega_{ci})}.
\end{aligned}
\tag{A.1}
$$

The sum in (A.1) is to be taken over all ion species, including impurities. The conditions $\epsilon_{\mathrm{S}} = n_{\parallel}^2$ and $\epsilon_{\mathrm{L}} = n_{\parallel}^2$ defining the location of the IIH resonance and L-cutoff can be re-written in a simpler form

$$
\sum_i \frac{f_i \mathcal{Z}_i}{\mathcal{Z}_i^2 - \tilde{\omega}_{\mathrm{S}}^2} = \alpha, \qquad\qquad \sum_i \frac{f_i}{\mathcal{Z}_i - \tilde{\omega}_{\mathrm{L}}} = \alpha,
\tag{A.2}
$$

by introducing the following notations for the ion species 'i': $X_i = n_i/n_e$, $f_i = Z_i X_i$ – the fraction of the replaced electrons, $\mathcal{Z}_i = Z_i/A_i$ – ratio of the charge number to the atomic mass; $\omega_{c\mathrm{H}} = eB/(m_{\mathrm{H}}c)$ – the cyclotron frequency of hydrogen ions that is

used for the frequency normalization ($\tilde{\omega} = \omega/\omega_{cH}$), $\omega_{pH} = \sqrt{4\pi n_e e^2/m_H}$ – the reference hydrogen plasma frequency (note n_e instead of n_H), $\tilde{n}_\parallel^2 = n_\parallel^2 - 1 - \omega_{pe}^2/\omega_{ce}^2$ – effective $n_\parallel^2$ if accounting for the small vacuum and electron contributions to the tensor component ϵ_S. Then, the small parameter appearing on the right-hand side of Eqs. (A.2), which describes the effect of finite n_{tor} on the location of the IIH resonance and L-cutoff, is given by $\alpha = (\omega_{cH}^2/\omega_{pH}^2)\,\tilde{n}_\parallel^2$.

By substituting $f_1 = 1 - f_2 - \sum\limits_{imp} f_{imp}$, it can be shown that Eqs. (A.2) are equivalent to the following ones

$$-\mathcal{Z}_1 + \frac{(\mathcal{Z}_1 - \mathcal{Z}_2)(\tilde{\omega}_S^2 + \mathcal{Z}_1\mathcal{Z}_2)}{\tilde{\omega}_S^2 - \mathcal{Z}_2^2} f_2 = \gamma_S,$$

$$\gamma_S = \alpha(\tilde{\omega}_S^2 - \mathcal{Z}_1^2) - \sum_{imp} \frac{(\mathcal{Z}_1 - \mathcal{Z}_{imp})(\tilde{\omega}_S^2 + \mathcal{Z}_1\mathcal{Z}_{imp})}{\tilde{\omega}_S^2 - \mathcal{Z}_{imp}^2} f_{imp}$$

(A.3)

and

$$-1 + \frac{\mathcal{Z}_1 - \mathcal{Z}_2}{\tilde{\omega}_L - \mathcal{Z}_2} f_2 = \gamma_L,$$

$$\gamma_L = \alpha(\tilde{\omega}_L - \mathcal{Z}_1) - \sum_{imp} \frac{\mathcal{Z}_1 - \mathcal{Z}_{imp}}{\tilde{\omega}_L - \mathcal{Z}_{imp}} f_{imp}.$$

(A.4)

The right-hand side of Eqs. (A.3) and (A.4) includes contributions due to finite n_{tor} and impurities. Neglecting those terms the well-known expressions for the IIH and L-cutoff frequencies are obtained

$$\tilde{\omega}_{S0} = \mathcal{Z}_2\sqrt{\frac{1 - (1 - \mathcal{Z}_1/\mathcal{Z}_2)f_2}{1 - (1 - \mathcal{Z}_2/\mathcal{Z}_1)f_2}} \approx$$

$$\approx \mathcal{Z}_2 + \frac{(\mathcal{Z}_1^2 - \mathcal{Z}_2^2)}{2\mathcal{Z}_1}f_2 - \frac{(\mathcal{Z}_1 + \mathcal{Z}_2)(\mathcal{Z}_1 - \mathcal{Z}_2)^2(\mathcal{Z}_1 - 3\mathcal{Z}_2)}{8\mathcal{Z}_1^2\mathcal{Z}_2}f_2^2,$$

$$\tilde{\omega}_{L0} = \mathcal{Z}_2 + (\mathcal{Z}_1 - \mathcal{Z}_2)f_2.$$

(A.5)

For a plasma consisting of N ion species with different Z/A ratios and if $n_{tor} \neq 0$, there are N different solutions for $\tilde{\omega}_S^2$ and $\tilde{\omega}_L$ satisfying Eqs. (A.3) and (A.4). Thus, in the general case the solutions has to be evaluated numerically. There is an artificial solution, which appears due to $\alpha \neq 0$ ($\tilde{\omega}_L \simeq -1/\alpha$, $\tilde{\omega}_S^2 \simeq -\mathcal{Z}_1/\alpha$), while the other $N - 1$ solutions represent IIH resonances and L-cutoffs associated with the minority ions and $N - 2$ impurity species. We are interested in the solutions for $\tilde{\omega}_S$ and $\tilde{\omega}_L$, which correspond to the minority ions and generalize Eqs. (A.5), aiming for identifying the influence of n_{tor} and impurities on that.

Omitting the comprehensive algebra, we provide the formula for L-cutoff valid up to quadratic terms in α and f_{imp}, including the cross-terms:

$$\tilde{\omega}_L = \tilde{\omega}_{L0} + \epsilon_L,$$

$$\epsilon_L = \left[k_{11}\alpha f_2(1 - f_2) + \sum_{imp} k_{12} f_2 f_{imp}\right] \times \left[1 + k_{21}\alpha + \sum_{imp} k_{22} f_{imp}\right],$$

(A.6)

where the parameters k_{ij} are given by

$$
\begin{aligned}
k_{11} &= (\mathcal{Z}_1 - \mathcal{Z}_2)^2, \\
k_{12} &= (\mathcal{Z}_1 - \mathcal{Z}_2)(\mathcal{Z}_1 - \mathcal{Z}_{\text{imp}})/(\tilde{\omega}_{\text{L0}} - \mathcal{Z}_{\text{imp}}), \\
k_{21} &= (\mathcal{Z}_1 - \mathcal{Z}_2)(1 - 2f_2), \\
k_{22} &= (\mathcal{Z}_1 - \mathcal{Z}_{\text{imp}})(\mathcal{Z}_2 - \mathcal{Z}_{\text{imp}})/(\tilde{\omega}_{\text{L0}} - \mathcal{Z}_{\text{imp}})^2.
\end{aligned}
\tag{A.7}
$$

The expression for the IIH resonance is more complicated since Eq. (A.3) is written for $\tilde{\omega}_{\text{S}}^2$ rather than $\tilde{\omega}_{\text{S}}$. In that case, it can be shown that

$$
\begin{aligned}
\tilde{\omega}_{\text{S}} &= \sqrt{\tilde{\omega}_{\text{S0}}^2 + \epsilon_{\text{S}}}\,, \\
\epsilon_{\text{S}} &= \left[k_{11}\alpha f_2(1 - f_2) + \sum_{\text{imp}} k_{12} f_2 f_{\text{imp}} \right] \times \left[1 + k_{21}\alpha + \sum_{\text{imp}} k_{22} f_{\text{imp}} \right]
\end{aligned}
\tag{A.8}
$$

is a high-accuracy quadratic approximation for $\tilde{\omega}_{\text{S}}$. The expansion coefficients k_{ij} for $\tilde{\omega}_{\text{S}}$ are given by

$$
\begin{aligned}
k_{11}\,\bar{\mathcal{Z}}_1^3 &= \mathcal{Z}_1\mathcal{Z}_2(\mathcal{Z}_1^2 - \mathcal{Z}_2^2)^2, \\
k_{12}\,\bar{\mathcal{Z}}_1^2 &= \mathcal{Z}_2(\mathcal{Z}_1^2 - \mathcal{Z}_2^2)(\mathcal{Z}_1 - \mathcal{Z}_{\text{imp}})(\tilde{\omega}_{\text{S0}}^2 + \mathcal{Z}_1\mathcal{Z}_{\text{imp}})/(\tilde{\omega}_{\text{S0}}^2 - \mathcal{Z}_{\text{imp}}^2), \\
k_{21}\,\bar{\mathcal{Z}}_1^2 &= (\mathcal{Z}_1^2 - \mathcal{Z}_2^2)(\mathcal{Z}_1 - (\mathcal{Z}_1 + \mathcal{Z}_2)f_2), \\
k_{22}\,\bar{\mathcal{Z}}_1 &= (\mathcal{Z}_1 - \mathcal{Z}_{\text{imp}})/(\tilde{\omega}_{\text{S0}}^2 - \mathcal{Z}_{\text{imp}}^2)^2 \cdot \left[(\tilde{\omega}_{\text{S0}}^2 - \mathcal{Z}_{\text{imp}}^2)(\tilde{\omega}_{\text{S0}}^2 + \mathcal{Z}_1\mathcal{Z}_{\text{imp}}) - \right. \\
&\quad \left. - \mathcal{Z}_{\text{imp}}(\mathcal{Z}_1 + \mathcal{Z}_{\text{imp}})(\tilde{\omega}_{\text{S0}}^2 - \mathcal{Z}_2^2) \right],
\end{aligned}
\tag{A.9}
$$

where $\bar{\mathcal{Z}}_1 = \mathcal{Z}_1 - (\mathcal{Z}_1 - \mathcal{Z}_2)f_2$. Note that Eqs. (A.6–A.9) are valid for an arbitrary number of impurity species, and include the impurity and n_{tor} contributions simultaneously.

Figure A1(a) shows the location of the IIH resonance and L-cutoff in pure (^{3}He)–H plasma as a function of the FW toroidal wavenumber (the other parameters correspond to those used in Fig. 1). Considering $k_\parallel \neq 0$, both the IIH resonance and L-cutoff shift towards the LFS, and the thickness of the evanescence layer gradually decreases. As Fig. A1(a) clearly illustrates, this shift is almost linear in α and thus quadratic in n_{tor}. Analytical approximations given by Eqs. (A.6–A.9) are shown in Fig. A1 with dots and are in excellent agreement with the numerical results for the whole range of experimentally relevant n_{tor}. The formulas (A.6–A.9) are in an almost perfect agreement with numerical results if also impurities are accounted for. Figure A1(b) is calculated for $n_{\text{tor}} = 27$ and illustrates further (almost linear) shift of the MC layer and L-cutoff towards the LFS if the beryllium concentration is increased in a (^{3}He)–H plasma. In contrast to the effect of n_{tor}, the width of the evanescence layer increases gradually with $X[\text{Be}]$.
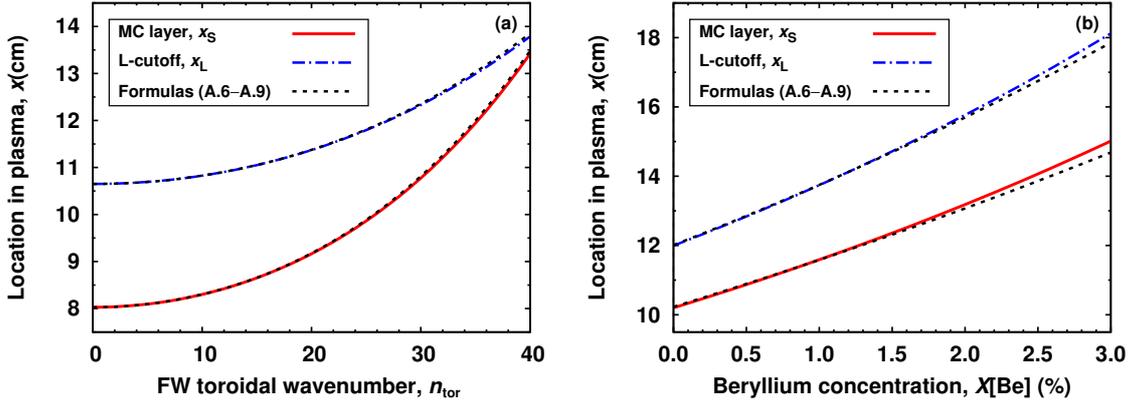
Figure A1. Location of the IIH resonance and L-cutoff in (^{3}He)–H plasma ($X[^3\text{He}] = 5.9\%$) as a function of the FW toroidal wavenumber (a), and beryllium concentration ($n_{\text{tor}} = 27$) (b).

If $f_2 \ll 1$ Eqs. (A.8) and (A.9) may be simplified by keeping in ϵ_S only the dominant terms in f_2:

$$
\begin{aligned}
\tilde{\omega}_S^2 &\approx \mathcal{Z}_2^2 + \frac{\mathcal{Z}_2(\mathcal{Z}_1^2 - \mathcal{Z}_2^2)}{\mathcal{Z}_1} f_2 + \frac{\mathcal{Z}_2(\mathcal{Z}_1 + \mathcal{Z}_2)(\mathcal{Z}_1 - \mathcal{Z}_2)^2}{\mathcal{Z}_1^2} f_2^2 + \\
&\quad + f_2 \left[k_{11}\alpha + \sum_{\text{imp}} k_{12} f_{\text{imp}} \right] \times \left[1 + k_{21}\alpha + \sum_{\text{imp}} k_{22} f_{\text{imp}} \right], \\
k_{11} &\approx \mathcal{Z}_2(\mathcal{Z}_1^2 - \mathcal{Z}_2^2)^2 / \mathcal{Z}_1^2, \\
k_{12} &\approx \mathcal{Z}_2(\mathcal{Z}_1^2 - \mathcal{Z}_2^2)(\mathcal{Z}_1 - \mathcal{Z}_{\text{imp}})(\mathcal{Z}_2^2 + \mathcal{Z}_1\mathcal{Z}_{\text{imp}})/(\mathcal{Z}_1^2(\mathcal{Z}_2^2 - \mathcal{Z}_{\text{imp}}^2)), \\
k_{21} &\approx (\mathcal{Z}_1^2 - \mathcal{Z}_2^2)/\mathcal{Z}_1, \\
k_{22} &= k_{12}k_{21}/k_{11} \approx (\mathcal{Z}_1 - \mathcal{Z}_{\text{imp}})(\mathcal{Z}_2^2 + \mathcal{Z}_1\mathcal{Z}_{\text{imp}})/(\mathcal{Z}_1(\mathcal{Z}_2^2 - \mathcal{Z}_{\text{imp}}^2)).
\end{aligned}
\tag{A.10}
$$

To the lowest order (linear in α and f_{imp}) we have

$$
\begin{aligned}
\tilde{\omega}_L &\approx \mathcal{Z}_2 + (\mathcal{Z}_1 - \mathcal{Z}_2)f_2 + (\mathcal{Z}_1 - \mathcal{Z}_2)^2 \alpha f_2 + \sum_{\text{imp}} \frac{(\mathcal{Z}_1 - \mathcal{Z}_2)(\mathcal{Z}_1 - \mathcal{Z}_{\text{imp}})}{\mathcal{Z}_2 - \mathcal{Z}_{\text{imp}}} f_2 f_{\text{imp}}, \\
\tilde{\omega}_S &\approx \mathcal{Z}_2 + \frac{\mathcal{Z}_1^2 - \mathcal{Z}_2^2}{2\mathcal{Z}_1} f_2 + \frac{(\mathcal{Z}_1^2 - \mathcal{Z}_2^2)^2}{2\mathcal{Z}_1^2} \alpha f_2 + \\
&\quad + \sum_{\text{imp}} \frac{(\mathcal{Z}_1^2 - \mathcal{Z}_2^2)(\mathcal{Z}_1 - \mathcal{Z}_{\text{imp}})(\mathcal{Z}_2^2 + \mathcal{Z}_1\mathcal{Z}_{\text{imp}})}{2\mathcal{Z}_1^2(\mathcal{Z}_2^2 - \mathcal{Z}_{\text{imp}}^2)} f_2 f_{\text{imp}}.
\end{aligned}
\tag{A.11}
$$

The first terms in Eqs. (A.11) show that both the IIH resonance and L-cutoff are located close to the minority IC layer. The second term illustrates a successive shift of the MC and L-cutoff layers towards the HFS or the LFS (depending on $\mathcal{Z}_1/\mathcal{Z}_2$ ratio) with increasing the concentration of minority ions. The third term corresponds to the contribution due to finite n_{tor}. It is always positive and, thus, accounting for $k_{\parallel} \neq 0$ results in a small shift of the layers towards the LFS. Finally, the fourth term represents the effect of impurities on the location of the layers in a plasma; its sign, which defines the direction of the additional shift due to impurities, depends on the sign of the ratio

$(\mathcal{Z}_1 - \mathcal{Z}_2)(\mathcal{Z}_1 - \mathcal{Z}_{\text{imp}})/(\mathcal{Z}_2 - \mathcal{Z}_{\text{imp}})$. Equation (A.11) for $\tilde{\omega}_\text{S}$ is used in the main text of the paper to evaluate the transition concentration of helium-3 ions in (^{3}He)–H plasma and the effect of impurities on that.

Appendix B. On '$\pm$' sign in formulas for the transition minority concentration

There is a simple physical explanation for the appearance of '$\pm$' sign in Eqs. (9) and (12) for the transition minority concentration. As mentioned in section 3, '+' or '−' sign is to be taken for the standard and inverted ICRH scenarios, respectively. In plasmas without impurities the IIH frequency is given by

$$\tilde{\omega}_\text{S} \approx \mathcal{Z}_2 + \frac{\mathcal{Z}_1^2 - \mathcal{Z}_2^2}{2\mathcal{Z}_1} f_2 + \frac{(\mathcal{Z}_1^2 - \mathcal{Z}_2^2)^2}{2\mathcal{Z}_1^2} \alpha f_2, \tag{B.1}$$

where $\alpha \propto (n_{\text{tor}}^2/n_e)(B/f)^2$. The sign of the second term in Eq. (B.1) is different for the standard ($\mathcal{Z}_1 < \mathcal{Z}_2$) and inverted ($\mathcal{Z}_1 > \mathcal{Z}_2$) ICRH scenarios. While for the standard scenarios the MC layer shifts towards the HFS with increasing the minority concentration, for the inverted scenarios it moves in the opposite (LFS) direction (Figure B1). At the same time the shift of the MC layer due to finite $k_\parallel$ (described by the third term in Eq. (B.1)) is always towards the LFS regardless the relation of Z/A ratio for majority and minority ions. Thus, for the inverted ICRH scenarios the shift of the MC layer due to X_2 and $k_\parallel$ is in the same direction, and therefore smaller minority concentration is needed for the MC layer to pass through the Doppler broadened minority IC region. Vice versa, for the standard scenarios the $k_\parallel$ correction counteracts the HFS shift of the MC layer with increasing X_2. This results in higher minority concentrations needed to pass the border, which marks the transition from MH to MC.
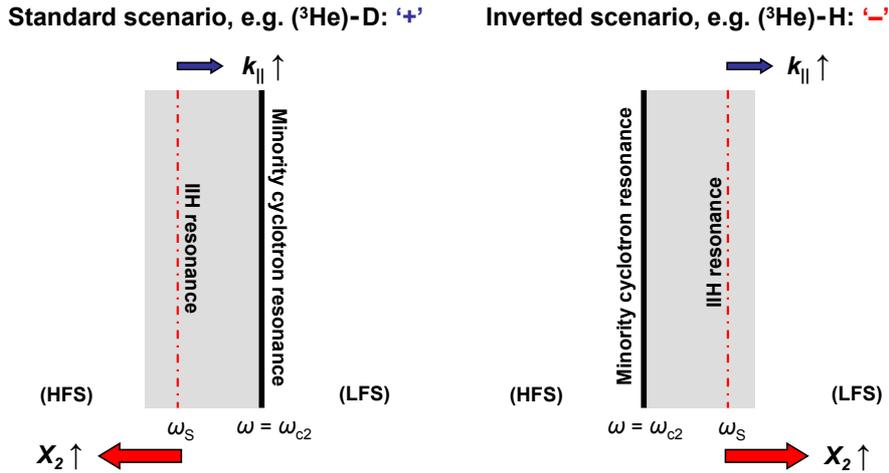
Figure B1. The shift of the IIH resonance with increasing X_2 and $k_\parallel$ is in the opposite/same direction for the standard/inverted ICRH scenarios, respectively. It results in a '$\pm$' sign that appears in the correction term for the transition minority concentration given by Eqs. (9) and (12).

References

[1] Mayoral M.-L., Colas L., Eriksson L.-G., Graham M., Ph. Jacquet, Lerche E., Monakhov I., Riccardo V., Van Eester D. and JET-EFDA Contributors 2011 *Proc. 19th Topical Conf. on RF Power in Plasmas (Newport, USA, 1–3 June 2011) AIP Conf. Proc.* **1406** 253–256.

[2] Gohil P., Jernigan T.C., Scoville J.T. and Strait E.J. 2009 *Nucl. Fusion* **49** 115004.

[3] Wesson J. 2004 *Tokamaks* (Oxford: Clarendon).

[4] Stix T.H. 1992 *Waves in Plasmas* (New York: AIP).

[5] Jaeger E.F., Berry L.A., Myra J.R., Batchelor D.B., D'Azevedo E., Bonoli P.T., Phillips C.K., Smithe D.N., D'Ippolito D.A., Carter M.D., Dumont R.J., Wright J.C. and Harvey R.W. 2003 *Phys. Rev. Lett.* **90** 195001.

[6] Mantsinen M.J. *et al* 2004 *Nucl. Fusion* **44** 33–46.

[7] Lerche E.A., Van Eester D. and JET EFDA contributors 2008 *Plasma Phys. Control. Fusion* **50** 035003.

[8] Majeski R. *et al* 1996 *Phys. Rev. Lett.* **76** 764–767.

[9] Becoulet A. 1996 *Plasma Phys. Control. Fusion* **38** A1–A12.

[10] Parisot A., Wukitch S.J., Bonoli P., Greenwald M., Hubbard A., Lin Y., Parker R., Porkolab M., Ram A.K. and Wright J.C. 2007 *Plasma Phys. Control. Fusion* **49** 219–235.

[11] Lin Y., Rice J.E., Wukitch S.J., Greenwald M.J., Hubbard A.E., Ince-Cushman A., Lin L., Porkolab M., Reinke M.L. and Tsujii N. 2008 *Phys. Rev. Lett.* **101** 235002.

[12] Lin Y. *et al* 2009 *Phys. Plasmas* **16** 056102.

[13] Hellsten T. *et al* 2012 *Plasma Phys. Control. Fusion* **54** 074007.

[14] Noterdaeme J.-M. *et al* 1999 *Proc. 26th EPS Conf. on Plasma Phys. (Maastricht, Netherlands, 14–18 June 1999)* 1561–1564.

[15] Mayoral M.-L. *et al* 2006 *Nucl. Fusion* **46** S550–S563.

[16] Lamalle P.U. *et al* 2006 *Nucl. Fusion* **46** 391–400.

[17] Van Eester D. *et al* 2012 *Plasma Phys. Control. Fusion* **54** 074009.

[18] Lerche E. *et al* 2012 *Plasma Phys. Control. Fusion* **54** 074008.

[19] Van Eester D. and Koch R. 1998 *Plasma Phys. Control. Fusion* **40** 1949–1975.

[20] Kazakov Ye.O., Kiptily V.G., Sharapov S.E., Van Eester D. and JET EFDA Contributors 2012 *Nucl. Fusion* **52** 094012.

[21] Hedin J., Hellsten T., Eriksson L.-G. and Johnson T. 2002 *Nucl. Fusion* **42** 527–540.

[22] Brambilla M. 1999 *Plasma Phys. Control. Fusion* **41** 1–34.

[23] Jucker M., Graves J.P., Cooper W.A. and Johnson T. 2011 *Plasma Phys. Control. Fusion* **53** 054010.

[24] Jaeger E.F. *et al* 2006 *Phys. Plasmas* **13** 056101.

[25] Dumont R.J. 2009 *Nucl. Fusion* **49** 075033.

[26] Budny R.V. *et al* 2012 *Nucl. Fusion* **52** 023023.

[27] Budden K.G. 1985 *The Propagation of Radio Waves* (Cambridge: Cambridge University Press).

[28] Majeski R., Phillips C.K. and Wilson J.R. 1994 *Phys. Rev. Lett.* **73** 2204–2207.

[29] Fuchs V., Ram A.K., Schultz S.D., Bers A. and Lashmore-Davies C.N. 1995 *Phys. Plasmas* **2** 1637–1645.

[30] Kazakov Ye.O., Pavlenko I.V., Van Eester D., Weyssow B. and Girka I.O. 2010 *Plasma Phys. Control Fusion* **52** 115006.

[31] Noterdaeme J.-M., Eriksson L.-G., Mantsinen M., Mayoral M.-L., Van Eester D., Mailloux J., Gormezano C. and Jones T.T.C. 2008 *Fusion Sci. Tech.* **53** 1103–1151.

[32] Shea D. and Morgan D. 2010 "The Helium-3 Shortage: Supply, Demand, and Options for Congress", Congressional Research Service, on-line: `www.fas.org/sgp/crs/misc/R41419.pdf`.

[33] Takahashi H. "ICRF heating in tokamaks" 1977 *J. Phys. Colloques (France)* **38 (C6)** 171–190, `http://dx.doi.org/10.1051/jphyscol:1977616`.

[34] Lashmore-Davies C.N., Fuchs V., Francis G., Ram A.K., Bers A. and Gauthier L. 1988 *Phys.*

Fluids **31** 1614–1622.

[35] Coenen J.W. *et al* "Longterm evolution of the impurity composition and impurity events with the ITER-like wall at JET" (submitted to *Nucl. Fusion*).

[36] Czarnecka A. *et al* 2012 *Proc. 39th EPS Conf. on Plasma Phys. (Stockholm, Sweden, 2–6 July 2012)* paper P5.047.

[37] Van Eester D. *et al* 2012 *Proc. 39th EPS Conf. on Plasma Phys. (Stockholm, Sweden, 2–6 July 2012)* paper P1.094.